SLAC-PUB-15612

Microwave instability of coasting ion beam with space charge in small isochronous ring

Yingjie Li*

Department of Physics, Michigan State University, East Lansing, MI 48824, USA

Lanfa Wang
SLAC National Accelerator Laboratory, Menlo Park, CA 94025, USA

(Dated June 12, 2013)

A novel coupling of the transverse betatron motion to the longitudinal microwave instability is studied. Besides the radial coherent dipole mode space charge field, simulation and theoretical studies in this paper show that the longitudinal coherent dipole mode space charge field due to deformation of beam shape also plays an important role in the isochronous regime, it induces betatron oscillation frequencies in temporal evolutions of growth rates spectra of longitudinal charge densities, radial offsets and energy deviations of local centroids, it makes the instantaneous instability growth rates dependent on both the amplitudes and phases of modulations of the above parameters. This paper also introduces a 2D dispersion relation incorporating the Landau damping effects due to finite energy spread and emittance, simulation results show it is more suitable for accurate prediction of the microwave instability growth rates than the conventional 1D growth rates formula. Nonlinear beam dynamics is also studied by co-rotational motion of two-macro-particle model in **E×B** field, energy spread measurements and simulations.

PACS numbers: 29.27.Bd, 29.20.dg

I. INTRODUCTION

In recent years, high power isochronous cyclotrons have been considered for applications in scientific research, medical therapy, etc. A bottleneck that limits the operation of a high power isochronous cyclotron is the beam instability induced by the space charge force. Gordon [1] explained the physical origin of vortex motion and deformation of beam shape in cyclotrons. In the last decade, additional extensive studies on the space charge effects in isochronous regime have been done through numerical simulations, experiments and analytical models [2-9].

Pozdeyev and Bi proposed their own models and theories to explain the mechanisms of microwave instability of a coasting beam with space charge in a circular accelerators operating in the isochronous regime [5-7], respectively. The two models only take into account the radial coherent dipole mode space charge field due to beam centroid wiggles and longitudinal monopole mode space charge field originating from line charge density modulations, none of them discusses the effects of longitudinal coherent dipole mode space charge field on evolution of beam instability due to beam shape deformation. The perturbation wavenumber k in Pozdeyev's model and growth rate formula [5, 6] is defined in the sinusoidal radial centroid offset function of a beam with uniform charge density, while in Bi's model and growth rate formula [7], the perturbation wavenumber k is defined in the line density modulation function, actually the growth rates spectra of the line charge densities and radial centroid offsets are different, the relation and interaction between the evolutions of two spectra of different meanings in physics are not discussed in the two models. The missing term of unperturbed line density in the calculation of radial coherent space charge field in [7] also makes the growth rates formula not compatible with the scaling law with respect to beam intensity observed in simulations and experiments [3, 5, 6]. Both models use 1D conventional growth rates formula derived exclusively for a mono-energetic beam, this may lead to the overestimation of instability growth rates, especially for the perturbation of short wavelengths, because the Landau damping effects caused by finite energy spread and emittance are all neglected.

Simulation studies in this paper show that the instantaneous microwave instability growth rates in isochronous regime are dependent on both the modulation amplitudes and phases of line charge densities, radial offsets and mean energy deviations of local centroids, the temporal evolutions of growth rates spectra of the above parameters are usually characterized by a betatron oscillation superimposed on exponential growths. These phenomena cannot be explained by the two models with conventional 1D microwave

Work supported in part by US Department of Energy under contract DE-AC02-76SF00515.

instability growth rate formula which can only predict a pure exponential growth. A theoretical discussion in this paper explains that the above novel beam behaviors primarily originate from the longitudinal coherent dipole mode space charge field of the deformed beam, the interaction and correlation of temporal evolutions of harmonic spectra between line charge densities, radial offsets and energy deviations of local centroids are also revealed by a set of longitudinal and radial equations of motion taking into account both the radial and longitudinal coherent dipole mode space charge fields.

To predict the microwave instability growth rates more accurately, this paper introduces and modifies a 2D dispersion relation [10] which incorporates the Landau damping effects contributed from finite energy spread and emittance. It can explain the suppression of microwave instability growth rates for short perturbation wavelengths and predict the fastest-growing wavelength. A simple example verification of Cerfon's theory of drift velocity in the **E**× **B** field [9] using two-macro–particle model is also provided in this paper, it simply explains the characteristic binary cluster merging phenomenon in isochronous rings; the simulation and experimental studies of energy spread evolution of a long coasting bunch show the energy spread of clusters changes slowly at large turn numbers, it may result from nonlinear advection of the beam in the **E**× **B** velocity field.

This paper is organized as follows. Sec. II gives a brief introduction to Small Isochronous Ring (SIR) and simulation code used. Simulation and theoretical studies of the temporal evolution of beam parameters affected by both longitudinal and radial coherent space charge field are provided in Sec. III and IV, respectively. The limits of conventional 1D growth rates formula is pointed out and a modified 2D dispersion relation with Landau damping effects for a Gaussian beam model is introduced in Sec. V. Sec. VI discusses the nonlinear beam dynamics by two-macro-particle model, energy spread measurements and simulations.

II. SMALL ISOCHRONOUS RING AND CYCO

To simulate and study beam dynamics of high power isochronous cyclotrons, a low energy, low beam Small Isochronous Ring (SIR) was constructed between 2001-2004 at the National Superconducting Cyclotron Lab (NSCL) at Michigan State University (MSU) as a thesis project for two graduate students and was in operation until 2010 [3-4]. The Small Isochronous Ring is designed to study space charge effects of H_2^+ ion beam with a typical kinetic energy of 20 keV, beam current of 5-25 uA, bunch length of 15 cm – 5.5 m, the radial and vertical tunes are 1.14 and 1.11, respectively, its bare slip factor is 2×10^{-4}. The Small Isochronous Ring consists of a multi-cusp Hydrogen ion source, injection line and storage ring. The ion source can produce three species of Hydrogen ions and an analyzing dipole magnet is used to select the H_2^+ ions which are usually used in the experiments. The H_2^+ ion beam with desired beam length can be produced by a chopper and its Courant-Snyder parameters may be matched to the storage ring by an electrostatic quadrupole triplet. The storage ring has a circumference of 6.58 meter, it mainly consists of four identical flat field bending magnets with edge focusing, and the 26^o pole face rotation angle of each magnet provides both vertical focusing and isochronism. After injection to the storage ring by a pair of fast pulsed electrostatic inflectors, the bunch can coast in the ring up to 200 turns. There is an extraction box located in the drift line between the 2^{nd} and 3^{rd} bending magnets, a pair of fast pulsed electrostatic deflector in the extraction box can kick the beam either up to a phosphor screen above the median ring plane, or down to the fast Faraday cup below the median ring plane. The phosphor screen and fast Faraday cup are used to monitor the transverse and longitudinal beam profiles, respectively. We can also perform energy spread measurement if the fast Faraday cup assembly is replaced by an energy analyzer assembly.

CYCO [3] is a 3D Particle-In-Cell (PIC) simulation code that is developed by Pozdeyev to study the beam dynamics with space charge in isochronous regime. It can numerically solve the complete and self-consistent system of six equations of motion of charged particles in a realistic 3D field map including space charge field. Because of large aspect ratio between the vacuum chamber width and height of the storage ring, the code only includes the image charge effects in the vertical direction, the rectangular vacuum chamber is simplified as a pair of infinitely large ideally conducting plates parallel to the median ring plane.

III. SIMULATION STUDIES ON EVOLUTIONS OF BEAM PARAMETERS IN ISOCHRONOUS RING

In order to acquire detailed information and properties of microwave instability evolution in isochronous ring accurately and comprehensively, in this section, we will present the simulation methods and results of exploring the beam parameter space in isochronous regime based on Fast Fourier Transformation (FFT) technique.

A. Effects of modulation strengths and phases on instantaneous instability growth rates

First, a default mono-energetic and straight H_2^+ bunch of beam intensity $I_0 = 10$ uA, kinetic Energy $E_{k0} = 19.9$ keV, bunch length $\tau_b = 300$ ns (~40 cm), radial and vertical emittance $\varepsilon_{x,0} = \varepsilon_{y,0} = 50\ \pi$ mm*mrad was created by CYCO. The initial bunch has a uniform distribution in both 4D transverse phase space (x, x', y, y') and longitudinal charge density. Then various beam parameter modulations are created as below:

(1) Line charge density modulation function:

$$\Lambda_1(k) = \hat{\Lambda}\cos(kz) \tag{1}$$

with modulation strength $S = \hat{\Lambda}/\Lambda_0 = 0$, 0.05, 0.1 and wavelength $\lambda = 2\pi/k = 2.0$ cm, Λ_0 is the unperturbed line charge density;

(2) Radial centroid offset modulation functions : (a) $x_c = a_c\cos(k_c z)$; (b) $x_c = -a_c\sin(k_c z)$ where $a_c = 0$, 0.05 mm, 0.1 mm, 0.2 mm, 0.5 mm, 1.0 mm and $\lambda_c = 2\pi/k_c = \lambda = 2.0$ cm.

(3) Coherent local kinetic energy deviation functions: (a) $\Delta E_c = 0$; (b) $\Delta E_c / E_{k0} = 2x_c / R$.

where $E_{k0} = 19.9$ keV, R is average ring radius. The second relation between ΔE_c and x_c satisfies isochronous condition of low energy SIR beam.

The code CYCO was run for a beam of initial distribution with some combinations of the above modulation parameters, the instantaneous instability growth rates of line charge density perturbation magnitude of wavelength $\lambda = 2$ cm at turn 0 are calculated by performing FFT analysis for the central part of beam profiles between turn 0 and turn 1 as shown in Figure 1.

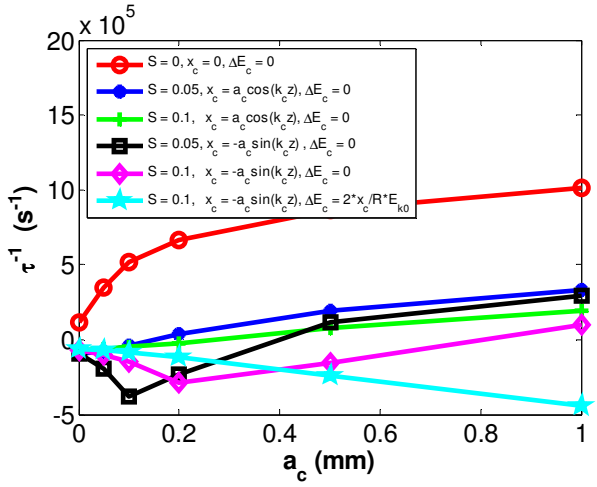

FIG. 1. (Color) Effects of modulation strengths and phases of various beam parameters on instantaneous beam instability growth rates.

Simulation results in Figure 1 indicate that both amplitudes and phases of line charge density modulation strengths, radial centroid offsets, and coherent local energy deviations may affect the instantaneous instability growth rates.

B. Betatron oscillations in long term instability growth curves

The simulation study of long-term linear stage of microwave instability was carried out by lowering the beam intensity in Sec. A to $I_0 = 1$ uA and keeping other beam parameters unchanged. Figure 2 shows the evolution of top view of beam profiles. The beam moves from left to right. We can observe the beam shape is deformed due to space charge force.

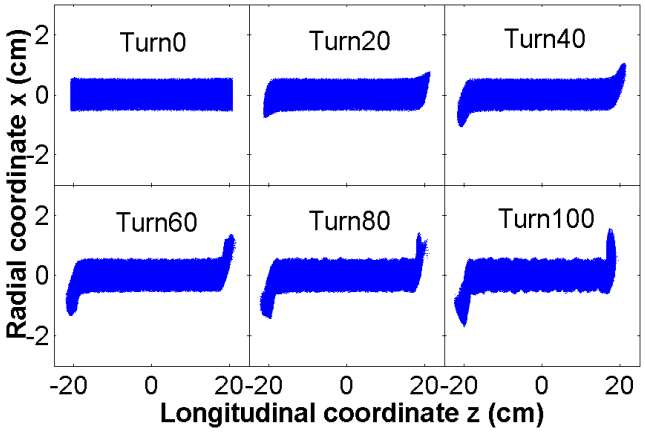

FIG. 2. (Color) Evolution of top view of beam profiles.

FFT analysis was performed for spectral evolutions of line charge densities, radial offsets and energy deviations of centroids with respect to longitudinal coordinate z, the analysis results of some chosen perturbation wavelengths are shown in Figure 3 - Figure 5, respectively.

It is clearly shown that there are many oscillations superimposed on the exponential growth curves in the figures. Because the radial betatron tune of SIR beam is 1.14, the betatron oscillation period is about $1/0.14 \approx 7$ turns, it is easy to judge that these oscillations are induced by the coupling of betatron oscillations. It is the first time to clearly observe this coupling to our knowledge. Actually, an indication of similar oscillations can be found in the Fig. 9 of [6], where there is a fast instability growth due to high beam intensity.

The beam behaviors in Sec. A and B cannot be explained by the existing models and theories, in fact, they are all caused by the longitudinal dipole mode space charge field due to beam deformation which will be explained in Sec. IV.

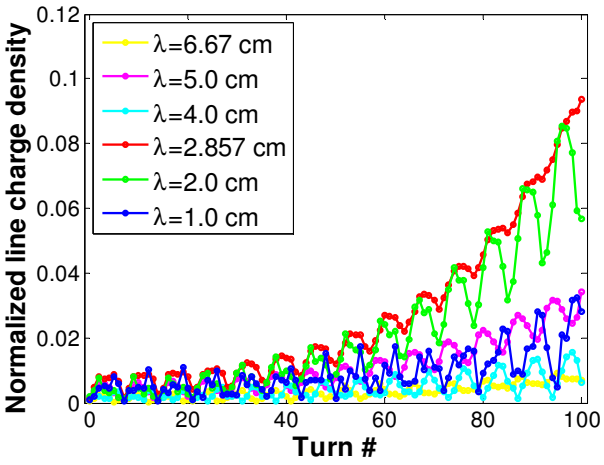

FIG. 3. (Color) Evolution of harmonic amplitudes of normalized line charge density.

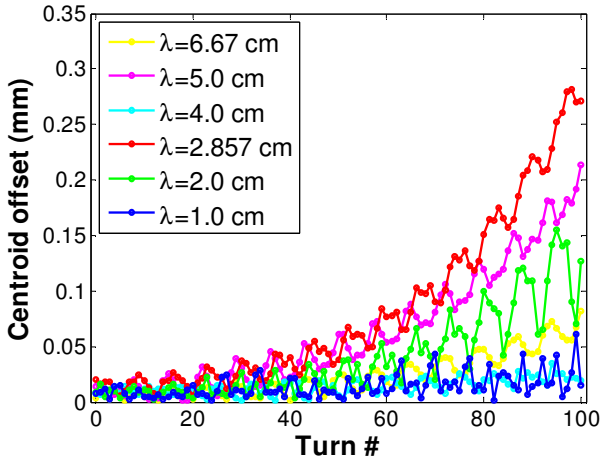

FIG. 4. (Color) Evolution of harmonic amplitudes of radial centroid offsets.

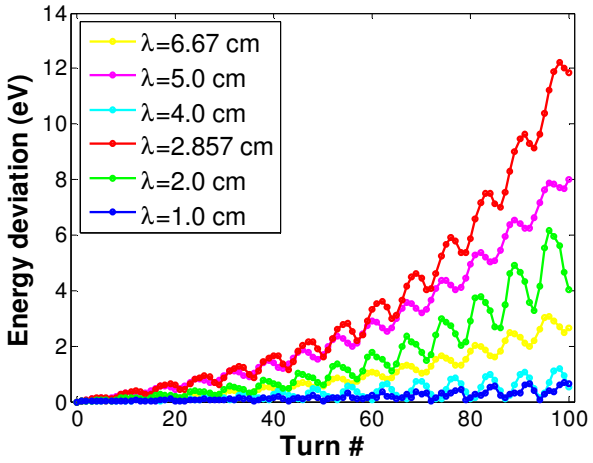

FIG. 5 (Color) Evolution of harmonic amplitudes of energy deviations.

IV. THEORETICAL STUDIES OF EVOLUTIONS OF BEAM PARAMETERS IN ISOCHRONOUS RING

In isochronous ring, the longitudinal line charge density gradient of a coasting bunch may induce energy deviations and the associated centroid offsets. For simplicity, we assume both centroid offset $x_c(z, t)$ and line charge density $\Lambda(z, t)$ consist of only a single harmonic component neglecting the nonlinear coupling between the chosen component with other components. For general purpose, we also assume there is no correlation between wavenumbers k_c of $x_c(z, t)$ and k of $\Lambda(z, t)$. Using the relation of phase $\Phi = ks - \omega t + \phi_0 = k(z + v_0 t) - \omega t + \phi_0 = kz - \omega t + kv_0 t + \phi_0$, where ϕ_0 is initial phase at t = 0, s = 0, $v_0 = \beta c$ is the velocity of on-momentum particles, then the local beam centroid $x_c(z, t)$, line charge density $\Lambda(z, t)$ and beam intensity I (z, t) can be expressed as:

$$x_c(z,t) = \hat{a}_c e^{j(k_c z - \omega t + \phi_c)} \tag{2}$$

$$\Lambda(z,t)=\Lambda_0+\Lambda_1(z,t)=\Lambda_0+\hat{\Lambda}e^{i(kz-\omega t+\phi)} \tag{3}$$

$$I(z,t)=I_0+I_1(z,t)=I_0+\hat{I}e^{i(kz-\omega t+\phi)} \tag{4}$$

where $\phi_c(t) = k_c v_0 t + \phi_{0,c}$, $\phi(t) = k v_0 t + \phi_0$, $\hat{I} = \hat{\Lambda}\beta c$, and amplitudes $\hat{a}_c$, $\hat{\Lambda}$, $\hat{I}$ are all real numbers. ω and ω_c are perturbation frequencies of line charge densities and radial centroid offsets, respectively.

A. **Longitudinal dipole mode coherent space charge field and impedance**

The centroid wiggles produce not only the radial dipole mode coherent space charge field E_x as pointed out by [6], but also its longitudinal counterpart $E_s^{(1)}$ as shown in Figure 6.

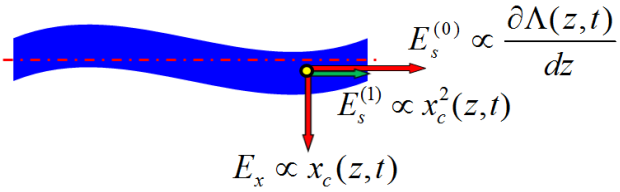

FIG. 6. (Color) Space charge components of local centroid with coordinate (x_c, z) at time t.

The total longitudinal space charge field on a local beam centroid can be approximated as:

$$E_s(z,t)=E_s^{(0)}(z,t)+E_s^{(1)}(z,t) \tag{5}$$

where the first and second terms in Eq. (5) are longitudinal space charge fields of monopole and dipole modes generated by line charge density modulations and centroid wiggles, respectively. If we adopt Pozdeyev's circular beam model of radius r_0 in free space [6], the first term of Eq. (5) can be calculated by setting r = 0 and $r_w = \infty$ in Eq. (17) of [7] as:

$$E_s^{(0)}(z,t)=-i\frac{\hat{\Lambda}e^{i(kz-\omega t+\phi)}}{\pi\varepsilon_0 r_0^2 k}[1-kr_0K_1(kr_0)] \tag{6}$$

The corresponding longitudinal monopole mode space charge impedance in low energy and short wavelength limit is [6]:

$$Z(k)=Z_{0,sc}^{\parallel}(k)=i\frac{2Z_0R}{k\beta r_0^2}[1-kr_0K_1(kr_0)] \tag{7}$$

Where Z_0= 377 Ω is the impedance in free space, r_0 is beam radius, k is charge density perturbation wave number, R is average ring radius, β is relativistic speed factor.

According to Eq. (4) of [6], the radial space charge field on a particle at coordinate (x, z) can be estimated in SI unit system as:

$$E_x(x,z,t) = \frac{\Lambda_0}{2\pi\varepsilon_0 r_0^{\,2}}[x - x_c(z,t)k_c r_0 K_1(k_c r_0)] \tag{8}$$

Where Λ_0 is the unperturbed part of line charge density, x_c (z, t) is the time-dependent local radial centroid offset. According to Panofsky-Wenzel theorem, the longitudinal dipole mode coherent space charge field on this particle can be calculated as:

$$E_s^{(1)}(x,z,t) = x\frac{\partial E_s(x,z,t)}{\partial x} = x\frac{\partial E_x(x,z,t)}{\partial z} = -\frac{\Lambda_0}{2\pi\varepsilon_0 r_0}k_c K_1(k_c r_0)x\frac{\partial x_c(z,t)}{\partial z} \tag{9}$$

Let $x = x_c$ in Eq. (9), with Eq. (2), the longitudinal space charge field of dipole mode becomes:

$$E_s^{(1)}(z,t) = -i\frac{\Lambda_0 \hat{a}_c^{\,2}}{2\pi\varepsilon_0 r_0}k_c^{\,2}K_1(k_c r_0)e^{2i(k_c z-\omega_c t+\phi_c)} \tag{10}$$

The dipole mode space charge wake potential over ring circumference C_0 [17, 18] is:

$$V = E_s^{(1)}(z,t)C_0 = -Z_{1,sc}^{\parallel} I_0 x_c^{\,2}(z,t) \tag{11}$$

From Eq. (10) and Eq. (11), the longitudinal dipole mode space charge impedance can be calculated as:

$$Z_{1,sc}^{\parallel} = i\frac{Z_0 R}{\beta r_0}k_c^{\,2}K_1(k_c r_0) \tag{12}$$

Figure 7 shows the longitudinal monopole and dipole mode space charge impedances of a circular H_2^+ beam with emittance of 50 π mm*mrad and kinetic energy of 19.9 keV in SIR.

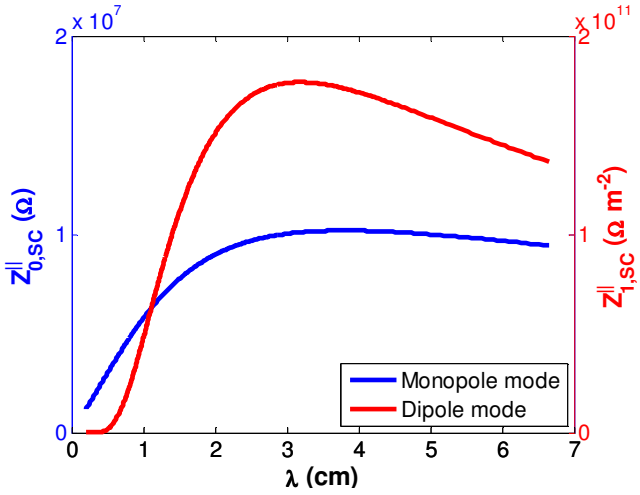

FIG. 7. (Color) Longitudinal monopole and dipole mode space charge impedances.

B. Radial and longitudinal equations of motion

According to Eqs. (5), (6) (10) and [17], the radial and longitudinal equations of motion of local beam centroid are:

$$x_c'' + \frac{v_{coh}^2(k_c)}{R^2} x_c = \frac{\delta_c}{R} \tag{13}$$

$$z' = -\eta \delta_c \tag{14}$$

$$\delta_c' = -i\frac{e\hat{\Lambda}e^{i(ks-\omega t+\phi_0)}}{\pi\varepsilon_0 r_0^2 k\beta^2 E}[1-kr_0K_1(kr_0)] - i\frac{e\Lambda_0\hat{a}_c^2}{2\pi\varepsilon_0 r_0\beta^2 E}k_c^2K_1(k_cr_0)e^{2i(k_cs-\omega_c t+\phi_{0,c})} \tag{15}$$

Where δ_c is the fractional momentum deviation of local beam centroid, ν_{coh} is the coherent radial betatron tune, η is slip factor, E is total energy. The prime stands for differentiation with respect to s. If δ_c (s = 0) = 0, then δ_c can be calculated by integration as:

$$\delta_c(s,t) = -\frac{e\hat{\Lambda}e^{i(ks-\omega t+\phi_0)}}{\pi\varepsilon_0 r_0^2 k^2\beta^2 E}[1-kr_0K_1(kr_0)] - \frac{e\Lambda_0\hat{a}_c^2}{4\pi\varepsilon_0 r_0\beta^2 E}k_cK_1(k_cr_0)e^{2i(k_cs-\omega_c t+\phi_{0,c})} \tag{16}$$

In the first order approximation, if centroid offset amplitude is small, the second term on RHS of Eq. (16) due to longitudinal dipole space charge field can be neglected, Eq. (13) becomes:

$$x_c'' + \frac{v_{coh}^2(k_c)}{R^2} x_c = -\frac{e\hat{\Lambda}e^{i(ks-\omega t+\phi_0)}}{\pi\varepsilon_0 r_0^2 k^2\beta^2 ER}[1-kr_0K_1(kr_0)] \tag{17}$$

We can see Eq. (17) describes a forced harmonic oscillation which results in $k \approx k_c$, $\omega \approx \omega_c$ and $\mathrm{Im}(\omega) \approx \mathrm{Im}(\omega_c)$, then in first order approximation, the growth rate spectra of line charge density modulations and local centroid offsets are approximately the same. If the second term on RHS of Eq. (16) is comparable to the first term thus cannot be neglected, then Eq. (17) will become a forced nonlinear second order differential equation and will not be discussed in this paper due to its complexity.

C. Betatron oscillations in evolution of beam parameters

If the longitudinal dipole mode coherent space charge field is taken into account, then we may define a time-dependent equivalent longitudinal monopole space charge field $[E_s^{(0)}(z,t)]_{eq}$ and equivalent longitudinal monopole space charge impedance $[Z_{0,sc}^{\parallel}(k,t)]_{eq}$ by Eq. (18) -Eq. (21) as below:

$$[E_s^{(0)}(z,t)]_{eq} = E_s^{(0)}(z,t) + E_s^{(1)}(z,t) \tag{18}$$

$$-E_s^{(0)}(z,t)C_0 = Z_{0,sc}^{\parallel}(k)\hat{I}e^{i(kz-\omega t+\phi)} \tag{19}$$

$$-E_s^{(1)}(z,t)C_0 = Z_{1,sc}^{\parallel}(k)I_0x_c^2(z,t) = Z_{1,sc}^{\parallel}(k)I_0\hat{a}_c^2e^{2i(k_cz-\omega_c t+\phi_c)} \tag{20}$$

$$-[E_s^{(0)}(z,t)]_{eq}C_0 = [Z_{0,sc}^{\parallel}(k,t)]_{eq}\hat{I}e^{i(kz-\omega t+\phi)} \tag{21}$$

Eq. (18) - Eq. (21) give:

$$[Z^{\parallel}_{0,SC}(k,t)]_{eq} = Z^{\parallel}_{0,sc}(k) + Z^{\parallel}_{1,sc}(k)\hat{a}_c^{\,2}\frac{I_0}{\hat{I}} e^{\mathrm{Im}[2\omega_c-\omega]t} e^{i[(2k_c-k)z-\mathrm{Re}[2\omega_c-\omega]t+(2\phi_c-\phi)]} \tag{22}$$

In the case of $k_c \neq k/2$, $[Z^{\parallel}_{0,sc}(k,t)]_{eq}$ will depend on longitudinal coordinate z, the beam dynamics is nonlinear, this complicated case will not be discussed in this paper.

In the case of $k_c = k/2$, $[Z^{\parallel}_{0,sc}(k,t)]_{eq}$ will be independent of longitudinal coordinate z, the dynamics is linear; Usually, $\mathrm{Re}(\omega_c) \approx \omega_\beta$, $\mathrm{Re}(\omega) \approx 0$, where ω_β is the angular betatron frequency. Then Eq. (22) can be simplified as:

$$[Z^{\parallel}_{0,sc}(k,t)]_{eq} = Z^{\parallel}_{0,sc}(k)[1 + Ae^{B(t)t}e^{-2i\omega_\beta t}] \tag{23}$$

where

$$A = \frac{Z^{\parallel}_{1,sc}(k)\hat{a}_c^{\,2}}{Z^{\parallel}_{0,sc}(k)}\frac{I_0}{\hat{I}} e^{i(2\phi_{0,c}-\phi_0)}, \tag{24}$$

$$B(t) = \mathrm{Im}[2\omega_c(t) - \omega(t)]. \tag{25}$$

Note A is a time-independent complex number, while B (t) is real and function of time t.

According to Eq. (3), the amplitude of perturbed line charge density can be expressed as:

$$|\Lambda_1(t)| = \hat{\Lambda} e^{\mathrm{Im}[\omega(t)]t} = \hat{\Lambda} e^{\frac{t}{\tau(t)}} \tag{26}$$

When energy spread, emittance and local centroid offsets are small, modulation wavelengths of line charge density are greater than beam diameter, the instability growth rates can be estimated by the conventional 1D microwave instability formula [6]:

$$\tau_0^{-1}(k) = \omega_0\sqrt{-i\frac{\eta e I_0 k R Z(k)}{2\pi\beta^2 E}} \tag{27}$$

Where ω_0 is the angular revolution frequency of on-momentum particles, e is unit charge, I_0 is unperturbed beam intensity. Z (k) is the longitudinal monopole mode space charge impedance which is given by Eq. (7) If $Z^{\parallel}_{0,sc}(k)$ of Eq. (27) is replaced by $[Z^{\parallel}_{0,sc}(k,t)]_{eq}$ of Eq. (23), the time-dependent growth rate becomes:

.

$$\tau^{-1}(k,t) = \tau_0^{-1}(k)\,\mathrm{Re}\{[1 + Ae^{B(t)t}e^{-2i\omega_\beta t}]^{\frac{1}{2}}\} \tag{28}$$

The amplitude of line charge density perturbation in Eq. (26) becomes:

$$|\Lambda_1(t)| = \hat{\Lambda} e^{\frac{t}{\tau_0(k)}\mathrm{Re}\{[1+Ae^{B(t)t}e^{-2i\omega\beta t}]^{\frac{1}{2}}\}} \tag{29}$$

If $\hat{a}_c = 0$, $|A| = 0$, $\tau^{-1}(k,t) = \tau_0^{-1}(k)$, $|\Lambda_1(t)| = \hat{\Lambda} e^{\frac{t}{\tau_0(k)}}$, it is a purely exponential growth as predicted by Eq. (27).

If $\hat{a}_c \neq 0$, $|A| \neq 0$ and $|Ae^{B(t)t}| << 1$, because $B(t) = \mathrm{Im}[2\omega_c(t) - \omega(t)] \approx \mathrm{Im}(\omega) = \tau_0^{-1}(k)$, Eq. (29) can be approximated as:

$$|\Lambda_1(t)| \approx \hat{\Lambda} e^{\frac{t}{\tau_0}} [1 + \sqrt{|A|} e^{\frac{t}{2\tau_0}} \cos(\omega_\beta t + \frac{\phi_0}{2} - \phi_{0,c})] \tag{30}$$

Eq. (30) is an exponential growth function modulated by betatron frequency ω_β, together with Eq. (17) and Eq. (16), the betatron frequencies in evolution of line charge densities, centroid offsets and energy deviations in Figure 3 - Figure 5 can be understood. From Eq. (30) and Eq. (24), we can see the instantaneous microwave instability growth rates depend on the current modulation strength $\hat{I} / I_0$, the centroid offset amplitude $\hat{a}_c$, the phase angles $\phi_{c,0}$ and ϕ_0, this characteristic property of beam profile evolution has already been observed in Figure 1 of Sec. III. Explanation of the dependence of instantaneous instability growth rates on coherent energy deviations $\Delta E_c / E_{k0}$ is not easy, it requires a more complicated formula than Eq. (27) which is only valid for 1D mono-energetic beam, this will not be discussed in this paper due to its complexity.

V. 2D DISPERSION RELATION

A. Limits of 1D growth rates formula

The transformation of longitudinal coordinate z is [10, 12]:

$$z = z_0 + R_{51} x_0 + R_{52} x_0' + R_{56} \delta \tag{31}$$

where $R_{51}(s)$, $R_{52}(s)$, and $R_{56}(s)$ are transfer matrix elements, x_0 and x_0' are radial coordinate and velocity slope, respectively; z is longitudinal coordinate with respect to bunch center, $\delta = \Delta p/p$ is fractional momentum deviation. For a beam in storage ring, $R_{56}(s)$ at $s = C_0$ is related to compaction factor α_c by [13]:

$$\alpha_c = -\frac{R_{56}(C_0)}{C_0} + \frac{1}{\gamma^2} = \frac{1}{C_0} \int_L \frac{D(s)}{R(s)} ds = < \frac{D(s)}{R(s)} > \tag{32}$$

where D(s) is local dispersion function, R(s) is local curvature of orbit, C_0 is the ring circumference. We can see Δz is determined by R_{51}, R_{52}, and R_{56} together. In the formalisms of [6] in which a conventional 1D growth rates formula Eq. (27) is adopted, only the contribution of compaction factor α_c or R_{56} to derivation of coherent slip factor η is considered. For a beam with small momentum spread δ (cold beam) and finite emittance, the term $R_{51}x_0 + R_{52}x_0$' may suppress the instability growth rates of short wavelengths thus should not be neglected.

B. 2D dispersion relation

For a hot beam, Landau damping effects due to emittance and energy spread are important, and a multidimensional dispersion relation including both longitudinal and transverse dynamics is needed [10,14,15]. For a coasting ultra-relativistic electron beam model whose initial equilibrium distributions in radial and longitudinal phase space are Gaussian functions, the 2D dispersion relation for CSR instability in storage ring in CGS unit was derived in Appendix B of [10] as:

$$1 = -\frac{ir_e n_b}{\nu^2 \gamma} kZ(k) \int_0^\infty ds e^{-\mu s} [s - \frac{R}{\nu} \sin \frac{\nu s}{R}] e^{-(k\sigma_x/\nu)^2[1-\cos(\nu s/R)] - (k\sigma_\delta/\nu^2)^2 \frac{s^2}{2}} \tag{33}$$

Where $r_e = e^2/mc^2$ is classical electron radius in CGS unit, γ is relativistic energy factor, ν is radial betatron tune, R is average ring radius in smooth approximation, Z(k) is CSR impedance with unit m^{-1}, σ_x is the RMS beam radius, σ_δ is the RMS uncorrelated energy spread of ultra-relativistic electrons. Eq. (33) is an integral equation which determines relation between k and μ. For a fixed k, μ can be solved numerically. If μ is real and $\mu>0$, the CSR instability grows at a rate of $\tau^{-1} = \mu\beta c$. Eq. (33) can be tailored to study microwave instability of non-relativistic H_2^+ beam of SIR induced by space charge after some modifications.

Eq. (1) and Eq. (4) of [10] should be modified as:

$$\frac{dz}{ds} = -\frac{x}{R(s)} \rightarrow -\frac{x}{R(s)} + \frac{\delta}{\gamma^2} \tag{34}$$

$$R_{56}(s) = -\int_0^s \frac{D(s')}{R(s')} ds' \rightarrow -\int_0^s \frac{D(s')}{R(s')} ds' + \frac{s}{\gamma^2} \tag{35}$$

Eq. (B4) of [10] should be modified as:

$$R_{56}(s,s') = -\frac{1}{\nu^2}(s-s') \rightarrow -(\frac{1}{\nu^2} - \frac{1}{\gamma^2})(s-s') \tag{36}$$

$$R_{56}(s' \rightarrow s) = -\frac{1}{\nu^2}[(s-s') - \frac{R}{\nu}\sin(\frac{\nu(s-s')}{R})] \rightarrow -(\frac{1}{\nu^2} - \frac{1}{\gamma^2})(s-s') + \frac{R}{\nu^3}\sin[\frac{\nu(s-s')}{R}] \tag{37}$$

The impedance and classical particle radius should be modified as:

$$Z = Z_{CSR}(k,s) \rightarrow \left(\frac{4\pi\varepsilon_0 c}{\beta C_0}\right) \frac{m_{e^-}}{m_{H_2^+}} Z_{0,SC}^{\parallel}(k) \tag{38}$$

$$r_e = \left(\frac{e^2}{m_{e^-} c^2}\right)_{CGS} \rightarrow \left(\frac{e^2}{4\pi\varepsilon_0 m_{H_2^+} c^2}\right)_{SI} \tag{39}$$

Where m_{e^-} and m_{H2}^+ are the rest masses of electron and H_2^+ ion, respectively.

Finally, the 2D dispersion relation in SI unit system for SIR beam becomes:

$$1 = -\frac{ie\Lambda_0}{\beta\gamma m_{H_2^+} c C_0} kZ_{0,SC}^{\parallel}(k) \int_0^\infty ds e^{-\mu s} [\left(\frac{1}{\nu_{coh}^2} - \frac{1}{\gamma^2}\right)s - \frac{R}{\nu_{coh}^2}\sin\frac{\nu_{coh} s}{R}]$$
$$e^{-(k\sigma_x/\nu_{inc})^2[1-\cos(\nu_{inc} s/R)] - \frac{1}{2}[k\sigma_\delta(1/\nu_{inc}^2 - 1/\gamma^2)s]^2} \tag{40}$$

Where Λ_0 is the unperturbed line charge density, c is the speed of light, $Z_{0,SC}^{\parallel}$ is the longitudinal space charge impedance in Ω, ν_c and ν_{inc} are coherent and incoherent radial betatron tunes modified by space charge effects, respectively.

Due to large ratios between vacuum chamber width, height and beam radius r_0, we can use Pozdeyev's model [6] of uniform circular beam with centroid wiggles in free space to calculate the radial space charge field and modified tunes. By smooth approximation and the equations of coherent and incoherent radial motions [6], the space-charge-modified coherent and incoherent betatron tunes can be derived easily as:

$$\nu_{coh} \approx 1 - \frac{\alpha_{coh}}{2}, \qquad \nu_{incoh} \approx 1 - \frac{\alpha_{incoh}}{2} \tag{41}$$

Where

$$\alpha_{coh} = \frac{e\rho_0}{2\varepsilon_0 m_{H_2^+}\omega_0^2}[1 - kr_0K_1(kr_0)], \qquad \alpha_{inc} = \frac{e\rho_0}{2\varepsilon_0 m_{H_2^+}\omega_0^2} \tag{42}$$

$\varepsilon_0 = 8.85\times10^{-12}$ F m^{-1} is permittivity of free space. ω_0 is angular revolution frequency of on-momentum particles, ρ_0 is volume charge density, $K_1(x)$ is the modified Bessel function of the second kind.

Thus if we neglect the transverse dynamics contributed from $R_{51}x_0$ and $R_{52}x_0$', the 1D slip factor is:

$$\eta_{SC}^{1D} = \frac{1}{v_{coh}^2} - \frac{1}{\gamma^2} \approx \alpha_{coh} = \frac{e\rho_0}{2\varepsilon_0 m_{H_2^+}\omega_0^2}[1 - kr_0K_1(kr_0)] \tag{43}$$

which is essentially the same as Eq. (12) derived in [6].

Using Eqs. (32)(37) (41-43), the 2D slip factor can be estimated as:

$$\eta_{SC}^{2D} = -\frac{R_{56}(0 \to C_0)}{C_0} = \left(\frac{1}{\nu_{coh}^2} - \frac{1}{\gamma^2}\right) - \frac{1}{2\pi\nu_{coh}^3}\sin(2\pi\nu_{coh}) \approx \frac{3}{2}\eta_{SC}^{1D} \tag{44}$$

For a mono-energetic beam, if we neglect the exponential damping term and the second term in the square bracket of integrand in Eq. (40), and use the equalities:

$$\int_0^\infty ds e^{-\mu s} s = \frac{1}{\mu^2}, \qquad \frac{1}{\nu_{coh}^2} - \frac{1}{\gamma^2} = \eta_{SC}^{1D} \tag{45}$$

the microwave instability growth rates $\tau^{-1}(k) = \mu\beta c$ predicted by Eq. (40) can be reduced to Eq. (27). We can see that the terms $R_{51}x_0$ and $R_{52}x_0$' can affect the microwave instability in isochronous ring in two ways: (a). Eq. (44) shows it can enhance the instability by increasing 50% of 1D slip factor derived in [6] (b). It provides Landau damping by the exponential suppression factor in Eq. (40).

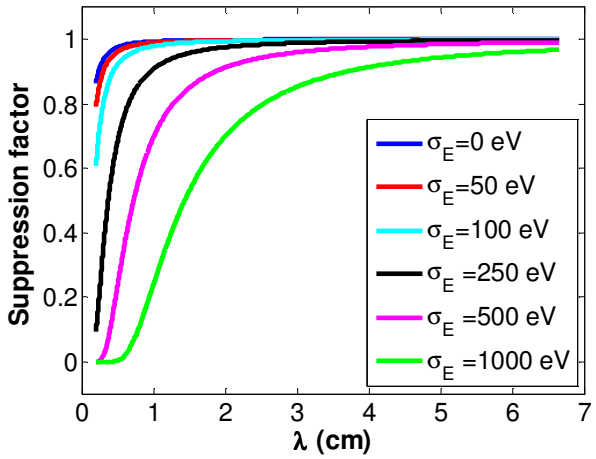

FIG. 8. (Color) Exponential suppression factor for a beam with current of 1uA, emittance of 50 π mm mrad and various RMS energy spread.

Figure. 8 shows the calculated exponential suppression factor in Eq. (40) for a beam with current of 1uA, emittance of 50 π mm mrad, mean kinetic energy of 19.9 keV and various uncorrelated RMS energy spread σ_E . We can see the Landau damping effects are more effective for smaller perturbation wavelengths.

C. Benchmarking of 2D dispersion relation

Note that the 2D dispersion relations Eq. (40) is derived for a Gaussian beam model without coherent radial centroid offsets and energy deviations, it is only valid for prediction of long term microwave instability growth rates in isochronous ring, not the instantaneous ones. We can fit the curves of line charge density evolution in Figure 3 to get simulated instability growth rates. If we replace t by $t = N_t T_0$, where N_t is the turn number, T_0 is the revolution period of H_2^+ ion, Eq. (30) may be expressed as a general fitting function below:

$$|\Lambda_1(N_t)| \approx \hat{\Lambda} e^{\frac{T_0}{\tau_0}N_t} + Pe^{QN_t}\cos(WT_0N_t + \Phi) \tag{46}$$

where $\hat{\Lambda}$, P, Q, W, Φ, τ_0 are fit coefficients, $1/\tau_0$ is just the long term instability growth rates.

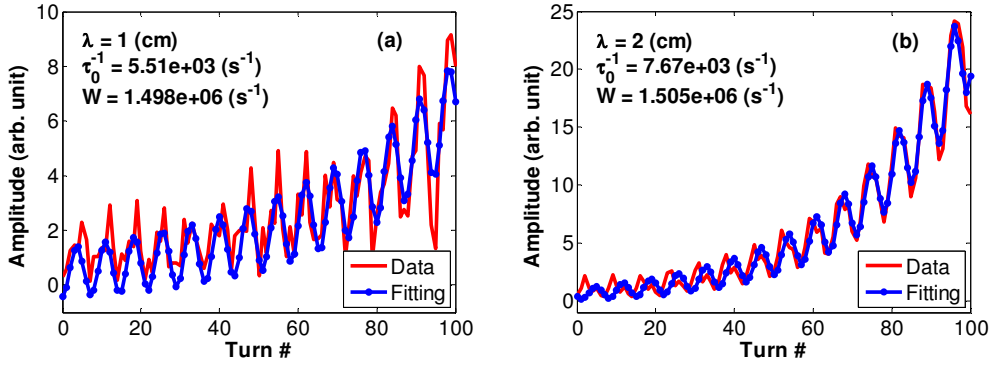

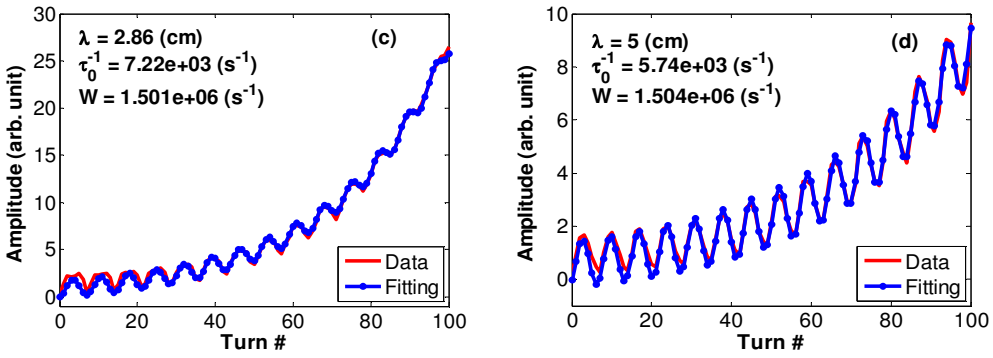

FIG. 9. (Color) Curve fitting results for growth rates of line charge densities

(a). λ = 1.0 cm; (b). λ = 2.0 cm; (c). λ = 2.86 cm; (d). λ = 5.0 cm;

The curve fitting results for growth rates of line charge densities of some chosen modulation wavelengths are show in Figure 9. For beam energy of 19.9 keV, the nominal angular betatron frequency is $\omega_\beta = 1.499 \times 10^6$ radian/second. We can see the oscillations in the curves are betatron oscillations. Figure 9 also shows that for $\lambda > 2.0$ cm, the linear effects of the centroid offset modulation wavelength $\lambda_c=2\lambda$ dominate over the nonlinear effects of $\lambda_c=\lambda$ on line density evolution; while for small wavelength $\lambda= 1.0$ cm, the nonlinear effects of the centroid offset modulations with wavelength $\lambda_c=\lambda$ on line density evolution are more noticeable.

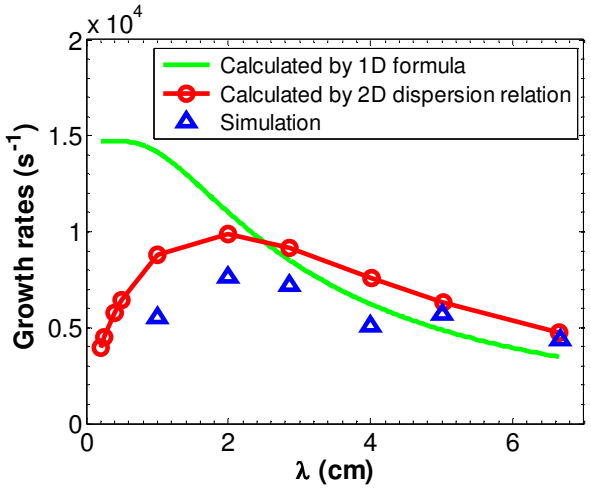

FIG. 10. (Color) Comparison of instability growth rates between theory and simulation.

Figure 10 shows the comparison of microwave instability growth rates between theoretical values predicted by 1D formula Eq. (27) with 1D slip factor expressed in Eq. (43), 2D dispersion relation Eq. (40), and simulation results by curve fitting for Figure 9. The 1D formalism overestimates the growth rates of short wavelengths and cannot predict the fastest-growing wavelength since Eq. (27) neglects the Landau damping effects, it also underestimates the growth rates of large wavelengths because the slip factor is underestimated as explained in Eq. (44). The 2D dispersion relation has a better performance than the conventional 1D formula, especially on the prediction of the growth rates of small wavelengths and the fastest-growing wavelength, because it includes the Landau damping effects. The difference of long term growth rates between theoretical predictions and simulations may originate from the emittance and energy spread growths of the coasting beam in simulations.

VI. NONLINEAR BEAM DYNAMICS OF SIR BUNCH

When a high intensity uniform long H_2^+ bunch of finite length is injected to SIR, the nonlinear space charge force on beam head and tail is very strong, in addition, the bunch may break up into many small clusters only after several turns of coasting due to microwave instability, the beam dynamics are highly nonlinear in these cases. In this section, we mainly discuss the two aspects of the nonlinear dynamics: (a). co-rotational motion in **E** × **B** field, (b). energy spread evolution.

A. Co-rotational motion in E × B field

Assume at t = 0, there are two identical macro-particles placed on the drift line between two ring bending magnets of SIR with initial distance d_0, each macro-particle has space charge Q and mass M which satisfies Q/M = e/m, where e and m are charge and mass of single H_2^+ ion, respectively. They have the same initial relativistic velocity $\beta_0 = 0.0033$ (corresponds to kinetic energy of 10.3 keV for H_2^+ ion), their initial moving directions are from left to right and are all parallel to the design orbit. If $Q = 8.0 \times 10^{-14}$ coulomb, $d_0 = 1.5$ cm, the top views of the two micro-particles are shown in Figure 11. This kind of co-rotational motion can be explained by Cerfon's theory of drift velocity in **E** × **B** field.

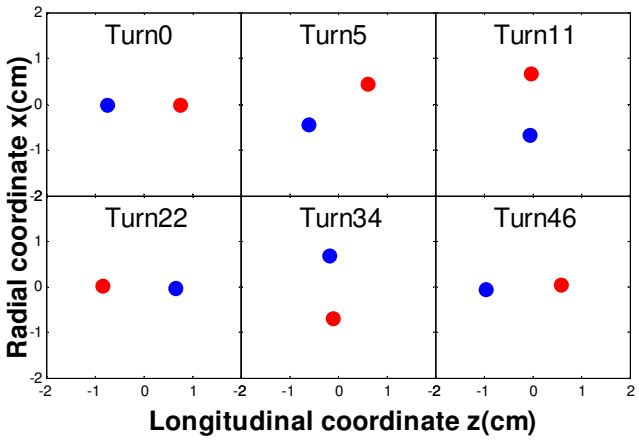

FIG. 11 (Color) Co-rotation of two-macro-particle model with $d_0 = 1.5$ cm.

Assume SIR can be simplified as an ideal circular storage ring of mean radius R with a uniform effective magnetic field of strength B_{eff}:

$$B_{eff} = \frac{mv_0}{eR} \tag{47}$$

where v_0 is the velocity of on-momentum particles, the magnetic field vector $\mathbf{B}_{eff}$ is perpendicular to and points into the paper. At time t the distance between them is d (t), the magnitude of space charge field $E_{s.c}$ on each macro-particle is:

$$E_{s.c} = \frac{Q}{4\pi\varepsilon_0 d^2(t)} \tag{48}$$

The space charge field vector $\mathbf{E}_{s.c}$ is along the line connecting the two macro-particles and points outward. Then each macro-particle will acquire a drift speed in their center of mass frame:

$$\vec{V}_{drift} = \frac{\vec{E}_{s.c} \times \vec{B}_{eff}}{B_{eff}^2} \tag{49}$$

which is perpendicular to both $\mathbf{B}_{eff}$ and $\mathbf{E}_{s.c}$, its magnitude is:

$$V_{drift} = \frac{E_{s.c}}{B_{eff}} = \frac{Q}{4\pi\varepsilon_0 B_{eff} d^2(t)} \tag{50}$$

If the trajectories of two particles are approximated as closed ellipses (actually their trajectories are complicated and not closed), their mean distance is estimated as <d> = (d_{min} + d_{max}) /2, then the angular frequency of co-rotation can be estimated as:

$$\omega_{co-rot.} = \frac{V_{drift}}{\frac{< d >}{2}} = \frac{Q}{2\pi\varepsilon_0 B_{eff} < d >^3} \tag{51}$$

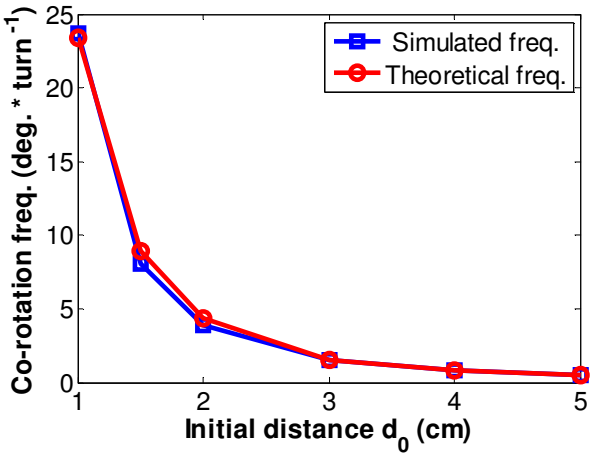

FIG. 12. (Color) Co-rotation frequencies of two-macro-particle model with different d_0.

By fitting slope of the curve of co-rotational angle v.s turn number in Figure 11, we can get the simulated co-rotational frequency. The simulated and theoretical co-rotation frequencies of the two-macro-particle model with Q = 8.0 × 10^{-14} coulomb, d_0 = 1.0 cm, 1.5 cm, 2.0 cm, 3.0 cm, 4.0 cm, and 5.0 cm are shown in Figure 12. We can see the simulated and theoretical values match quite well which verified Cerfon' theory, in fact, this two-macro-particle model may also help us understand the characteristic binary cluster merging phenomenon in isochronous ring.

B. Energy spread measurements and simulations

The evolution of beam energy spread of coasting bunch induced by space charge field plays an important role in both linear and nonlinear regime of beam instability. In linear beam dynamics, a large energy spread may help suppress the microwave instability; in nonlinear beam dynamics, the energy spread is one of important measures of asymptotic bunch behavior. In this section, we discuss the energy spread evolution by both simulation and experimental methods.

SIR Lab has designed a compact electrostatic retarding field analyzer [19] which can scan across the beam radially to measure the energy spread of a bunch at various chosen number of turns after injection. The analyzer is roughly a cube with a 1 mm (width) × 14 mm (height) entrance slit located in the middle of the entrance plate. It mainly consists of a rectangular housing tube, a rectangular high voltage retarding tube, a fine retarding mesh (1000 lines per inch, 50% transmission rates), a secondary electron suppressor, and a current collector. The analyzer is installed under the median ring plane in the extraction box, its entrance plate is tilted at an angle with respect to vertical plane to align the analyzer axis parallel to that of deflected beam. A pair of high voltage pulsed electrostatic deflector is used to kick the beam down to the energy analyzer when energy spread measurement is performed. Usually, the energy spread is measured at three radial positions: one is at the location of the peak beam current, and the other two positions are close to the beam core edges on each side.

A H_2^+ ion bunch of length 600 mm, peak current 8.0 uA, kinetic energy 10.3 keV and emittance 30 π mm mrad is used in the energy spread measurements. A mono-energetic macro-particle bunch of the above initial parameters with uniform distribution in both longitudinal line charge density and 4D transverse phase space are also used in the simulation study by code CYCO. In the analysis of simulation results, the radial beam size is cut into several 1 mm wide small bins, the number of macro-particles, mean kinetic energy and RMS energy spread in each bin are calculated and compared with experimental values. Figure 13 shows the simulated and experimental radial slice beam density. Figure 14 shows the simulated top view and RMS slice energy spread at turn 4. Figure 15 shows the simulated RMS slice energy spread up to turn 8. Figure 16 shows the simulated top view and RMS slice energy spread at turn 30. Figure 17 shows the comparison of RMS slice energy spread between simulations and experiments. Note that in this paper the slice energy spread and slice density denote all the slices are cut parallel to the longitudinal z direction instead of the radial direction that is conventionally used in FEL. Considering the charged long bunch is a chaotic system, a small difference in the initial beam distribution may cause huge beam profile deviation at large turn numbers, we can see that the simulated radial beam density profiles and RMS slice energy spread match the experimental values within an acceptable range.

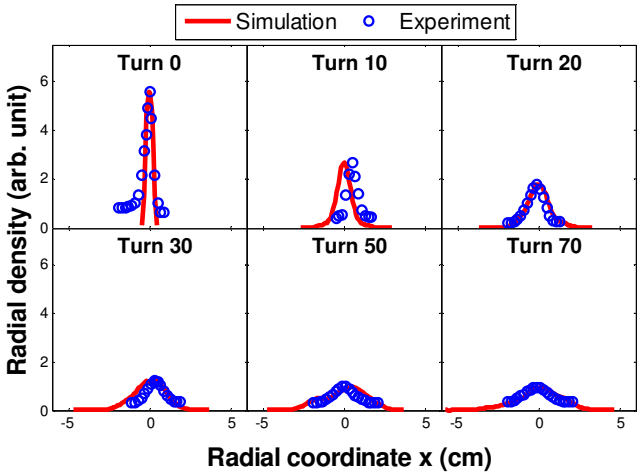

FIG. 13. (Color) Evolution of radial beam density.

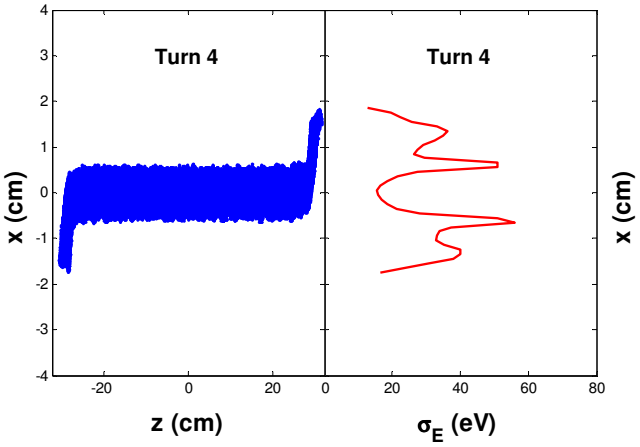

FIG. 14. (Color) Simulated top view (left) and RMS slice energy spread (right) at turn 4.

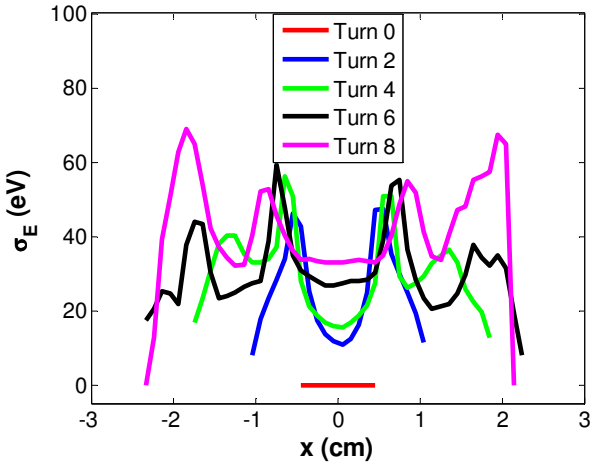

FIG. 15. (Color) Simulated RMS slice energy spread of turns 0-8.

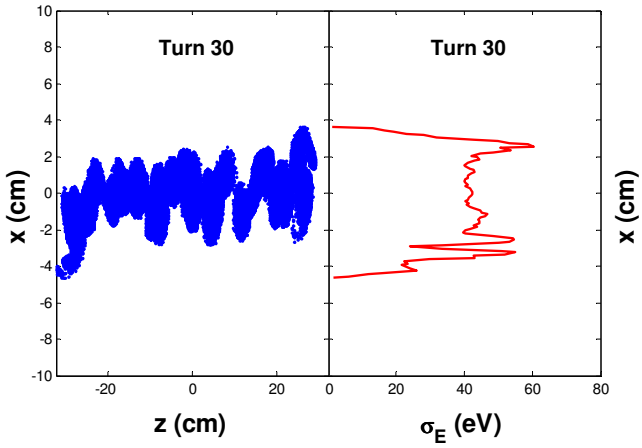

FIG. 16. (Color) Simulated top view (left) and RMS slice energy spread (right) at turn 30.

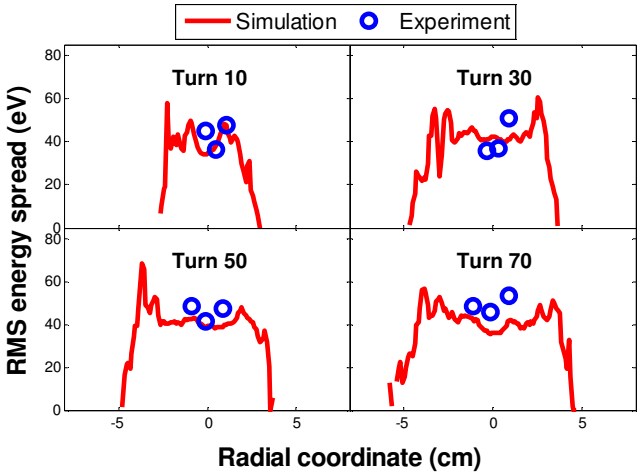

FIG. 17. (Color) Comparison of RMS slice energy spread.

Figure 13 - Figure 17 show that when an initially mono-energetic, straight long beam coasts in the isochronous ring, the space charge will induce the longitudinal density modulations and energy spread, at smaller turn numbers, the energy spread in beam head and tail is much greater than that of beam core around beam axis, as turn number increases, the radial RMS slice energy spread distribution tends to become uniform and changes very slowly. At the same time, the radial beam size increases, the beam centroids deviate from the design orbit. The beam centroid wiggles may also cause the difference in betatron oscillation phases between beam clusters (slices), if the beam is long enough, the radial centroid offsets of different clusters (slices) may be regarded as distributed randomly and uniformly around the design orbit, then the measured RMS slice energy spread at different radial coordinates is just the density weighted mean RMS slice energy spread of beam core of any individual cluster (slice) thus is independent of the radial coordinates. This can be explained below in Figure 18.

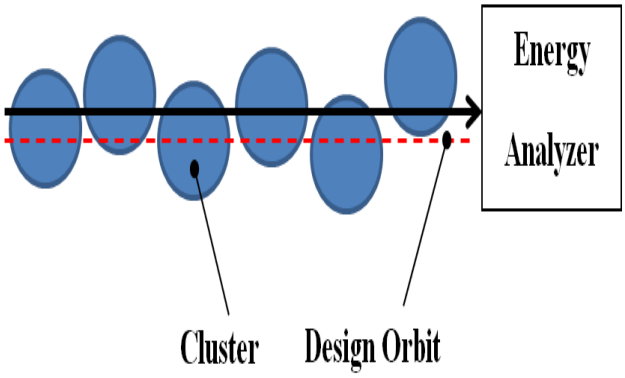

FIG. 18 (Color) Sketch of clusters and energy analyzer.

Figure 18 shows the long bunch has broken up into many identical small clusters (blue ovals) whose centroids distribute randomly and uniformly around the design orbit (the red dashed line). If we measure the RMS slice energy spread at a radial position as indicated by the solid black line with arrow, the analyzer will sample slices of different clusters. Let's assume there are N_c clusters in the whole bunch which are tagged by ID# 1, 2, 3 ,….N_c, each cluster has the same total particle number and radial charge distribution profile, if the slice sampled by the analyzer in each cluster contains n_i (i = 1, 2, 3,….N_c) charged particles and its RMS energy spread is σ_i, the mean kinetic energy of all slices are the same as $< E(x) >$ at large turn numbers, where x is the radial coordinate of black solid line with respect to the red dashed line, then the RMS energy spread in the i^{th} beam slice is:

$$\sigma_i = \sqrt{\frac{1}{n_i}\sum_{j=1}^{n_i}[E_j - < E(x) >]^2} \qquad (i=1, 2, 3,\ldots\ldots N_c) \tag{52}$$

The sum of square of Eq. (52) gives:

$$\frac{n_1\sigma_1^{\,2} + n_2\sigma_2^2 + \ldots\ldots n_{N_c}\sigma_{N_c}^2}{n_1 + n_2 + \ldots\ldots n_{N_c}} = < E_i^{\,2} > - < E(x) >^2 = \sigma_E^2(x) \tag{53}$$

$$\sigma_E(x) = [\frac{n_1\sigma_1^{\,2} + n_2\sigma_2^2 + \ldots\ldots n_{N_c}\sigma_{N_c}^2}{n_1 + n_2 + \ldots\ldots n_{N_c}}]^{\frac{1}{2}} \tag{54}$$

The RHS of the Eq. (54) is the weighted mean RMS energy spread of the sampled beam slices of different cluster cores at a fixed radial coordinate x, if the number of clusters is large enough and the radial centroid offsets of all the clusters are randomly and uniformly distributed around the design orbit, it is actually equal to the weighed mean RMS slice energy spread of any given single cluster core thus is independent of the coordinate x. In real measurements, the above ideal preconditions are not satisfied completely, there are always small energy spread fluctuations between different radial measurement points.

The equilibrium value of kinetic energy deviation $\Delta E_{eq}(x) = E_{eq}(x) - E_{k0}$ and radial coordinate x of an off-momentum particle satisfies the relation:

$$\Delta E_{eq}(x) = \frac{2E_{k0}}{R}x \tag{55}$$

Where $E_{eq}(x)$ is the equilibrium kinetic energy and is equal to <E(x)> of beam slices centered at x at large turn numbers. For simplicity, assume the radial beam density distribution is uniform, then the RMS energy spread of the equilibrium particles measured by SIR energy analyzer with an entrance slit of width Γ = 1 mm centered at x can be estimated as:

$$\sigma_{E_{eq}} = [\frac{1}{\Gamma}\int_{x-\frac{\Gamma}{2}}^{x+\frac{\Gamma}{2}}[\frac{2E_{k0}}{R}(x'-x)]^2 dx']^{\frac{1}{2}} = \frac{E_{k0}\Gamma}{\sqrt{3}R} \approx 5.7eV \tag{56}$$

This value is proportional to slit width Γ and is independent of x, it is much less than the asymptotic energy spread of about 50 eV at large turn numbers. It indicates that the number of particles of equilibrium energy only accounts for a small fraction of total particles in a beam slice.

The saturation of RMS slice energy spread of clusters in SIR is an indication of formation of nonlinear advection of the beam in the **E** × **B** velocity field. Assume an ideal disk-shaped cluster coasts in an isochronous ring of effective uniform magnetic field $\mathbf{B}_{eff}$, the $\mathbf{E}_{sc} \times \mathbf{B}_{eff}$ velocity field at any point of median plane inside the cluster is along the tangential direction in the rest frame of the cluster, no particles stay at the beam head (tail) forever, then the energy spread within a given beam slice of 1 mm width at any coordinate x will not build up with time significantly. During the binary cluster merging process, the total charge and size of new clusters grow at the same time, the mean charge density does not change considerably which may result in the saturation of mean RMS slice energy spread averaged along radial coordinate.

VII. CONCLUSION

In this paper we discussed the limits of two beam models on microwave instability and explore novel beam dynamics with space charge in isochronous regime. By simulation studies, we found the instantaneous microwave instability growth rates depend on not only the amplitudes of Fourier components of line charge densities, coherent local centroid offsets and energy deviations, but also their phases; the betatron oscillations in the growth rate spectra of above beam parameters are discovered, these phenomena were explained by longitudinal dipole mode coherent space charge field with the concept of time-dependent equivalent longitudinal space charge impedance for the case of k_c= k/2. This paper shows that for a long coasting bunch of space charge in isochronous regime, both the radial and longitudinal coherent space charge field should be taken into account in the beam dynamics. The growth rates spectra of line charge densities, local centroid offsets and energy deviations may interact each other and evolve in a self-consistent way.

In addition, by introducing a modified 2D dispersion relation, the Landau damping effects provided by finite emittance and energy spread are included in the beam dynamics, this is especially important for the accurate prediction of instability growth rates of short perturbation wavelengths and fastest-growing wavelength. Simulation results for long term instability growth rates show that the 2D dispersion relation has a better performance than the conventional 1D instability growth rate formula.

An accurate prediction of instantaneous instability growth rates in isochronous regime requires a more complicated 2D dispersion relation which derived for a beam with initial modulations in both coherent radial offsets and energy deviations of local centroids, it will be discussed in the future works.

We use a two-macro-particle model to test the theory of drift velocity in $\mathbf{E} \times \mathbf{B}$ field proposed by Cerfon. The good agreement between simulated and theoretically predicted co-rotation frequencies provides a good example to validate Cerfon's theory and assumptions; this model may also help us understand the approaching stage of the characteristic binary cluster merging phenomenon in isochronous ring.

The measured and simulated RMS slice energy spread and radial density profiles of a long coasting bunch reaches acceptable agreement, at smaller turn numbers, due to finite bunch length, the energy spread of beam head and tail dominates over that of the central part of bunch; while at large turn numbers, the randomly distributed cluster centroid offsets tend to make radial energy spread distribution of whole bunch uniform; the measured energy spread is just the density weighted mean RMS slice energy spread of any single cluster core, its saturation behavior indicates the formation of nonlinear advection of the particles due to the $\mathbf{E} \times \mathbf{B}$ velocity field in each cluster, during the successive binary cluster merging process of a long bunch, the mean RMS slice energy spread averaged over radial coordinate of merger remnants of parent cluster pairs with different sizes reaches an asymptotic value.

ACKNOWLEDGEMENTS

We would like to thank the guidance of Prof. F. Marti and T. P. Wangler, we are also grateful to Y.C. Wang, S. Y. Lee, K. Y. Ng, G. Stupakov, E. Pozdeyev, A. W. Chao, R. York, M. Syphers, V. Zelevinsky, J. Baldwin, and J. A. Rodriguez for their fruitful discussions and suggestions. This work was supported by NSF Grant # PHY 0606007.

REFERENCE

[1] M. M. Gordon, *Proceedings of the 5th International conference on Cyclotrons* (Oxford, United Kingdom, 1969), p. 305.
[2] S. A. Bogacz*, Proceedings of the IEEE Particle Accelerator Conference* (San Francisco, CA, U.S.A, May 6-9, 1991), p. 1815.
[3] E. Pozdeyev, Ph.D. thesis, Michigan State University (2003).
[4] J. A. Rodriguez, Ph.D. thesis, Michigan State University (2004).
[5] E. Pozdeyev, J. A. Rodriguez, F. Marti, R. C. York, *Proceedings of Hadron Beam* (Nashville, Tennessee, U.S.A, 2008), WGA30, p. 157.
[6] E. Pozdeyev, J. A. Rodriguez, F. Marti, R.C. York, Phys. Rev. ST Accel. Beams **5**, 054202 (2009).
[7] Y. Bi, T. Zhang, C. Tang, Y. Huang, J. Yang, J. Appl. Phys. **107**, 063304 (2010).
[8] C. Baumgarten, Phys. Rev. ST Accel. Beams **14**, 114201 (2011).
[9] A. J. Cerfon, J. P. Freidberg, F. I. Parra, T. A. Antaya, Phys. Rev. ST Accel. Beams **16,** 024202 (2013).
[10] S. Heifets, G. Stupakov, and S. Krinsky, Phys. Rev. ST Accel. Beams **5**, 064401 (2002).
[11] M. Venturini, Phys. Rev. ST Accel. Beams **11**, 034401 (2008).
[12] D. Ratner, A. Chao, Z. Huang, SLAC-PUB-13392.
[13] D.A. Edwards, M. J. Syphers, *An Introduction to the Physics of High Energy Accelerators* (John Wiley and Sons, New York, 1993).
[14] A. Marinelli and J. B. Rosenzweig, Phys. Rev. ST Accel. Beams **13**, 110703 (2010).
[15] A. Marinelli, E. Hemsing, and J. B. Rosenzweig, Phys. Plasmas **18**, 103105 (2011).
[16] M. Reiser, *Theory and Design of Charged Particle Beams*, 2nd edition (Wiley-VCH, 2008).
[17] A. W. Chao, *Physics of Collective Beam Instabilities in High Energy Accelerators* (Wiley Series in Beam Physics, 1993).
[18] K. Y. Ng, *Physics of Intensity Dependent Beam Instabilities* (World Scientific Publishing Co. Pte. Ltd, 2006).
[19] Y. Li, G. Machicoane, F. Marti, T. P. Wangler, E. Pozdeyev, *Proceedings of the IEEE Particle Accelerator Conference* (Vancouver, BC, Canada, 2009), TU3PBC06, p. 734.

FIG. 1. (Color) Effects of modulation strengths and phases of various beam parameters on instantaneous beam instability growth rates.

FIG. 2. (Color) Evolution of top view of beam profiles.

FIG. 3. (Color) Evolution of harmonic amplitudes of normalized line charge density.

FIG. 4. (Color) Evolution of harmonic amplitudes of radial centroid offsets.

FIG. 5 (Color) Evolution of harmonic amplitudes of energy deviations.

FIG. 6. (Color) Space charge components of local centroid with coordinate (x_c, z) at time t.

FIG. 7. (Color) Longitudinal monopole and dipole mode space charge impedances.

FIG. 8. (Color) Exponential suppression factor for a beam with current of 1uA, emittance of 50 π mm mrad and various RMS energy spread.

FIG. 9. (Color) Curve fitting results for growth rates of line charge densities

(a). λ = 1.0 cm; (b). λ = 2.0 cm; (c). λ = 2.86 cm; (d). λ = 5.0 cm.

FIG. 10. (Color) Comparison of instability growth rates between theory and simulation.

FIG. 11 (Color) Co-rotation of two-macro-particle model with d_0 =1.5 cm.

FIG. 12. (Color) Co-rotation frequencies of two-macro-particle model with different d_0.

FIG. 13. (Color) Evolution of radial beam density.

FIG. 14. (Color) Simulated top view (left) and RMS slice energy spread (right) at turn 4.

FIG. 15. (Color) Simulated RMS slice energy spread of turns 0-8.

FIG. 16. (Color) Simulated top view (left) and RMS slice energy spread (right) at turn 30.

FIG. 17. (Color) Comparison of RMS slice energy spread.

FIG. 18 (Color) Sketch of clusters and energy analyzer.